Supporting Information

Carbon vacancy defect-activated Pt cluster for hydrogen generation

Xiaobing Bao,[a] Yutong Gong,*[a] Yuzhuo Chen,[a] Hao Zhang,[b] Zhe Wang,[a] Shanjun Mao,[a] Lei Xie,[a] Zheng Jiang*[b] and Yong Wang*[a]

Table of the contents

Experimental Procedures

Materials.

Preparation of series of CNTs supports.

Preparation of Pt-based electrocatalysts.

Characterization.

Electrochemical measurements.

The estimation of active sites density (n) and turnover frequency (TOFs).

XAFS measurements and data processing.

Computational Methods and Models.

Results and Discussion

Figure S1 Charge distribution mapping of four types of carbon supports.

Figure S2 Morphology of pristine CNTs.

Figure S3 Textural properties of pristine CNTs.

Figure S4 HAADF-STEM image and HRTEM images of Pt/CNTs-ECR.

Figure S5 HAADF-STEM image and HRTEM images of Pt/CNTs-CR.

Figure S6 The proposed processes of Pt nucleation and growth for three different methods.

Figure S7 X-ray diffraction (XRD) analysis of Pt/CNTs-ECR and Pt/CNTs-CR.

Figure S8 The thermal stability of Pt/CNTs-ECR.

Figure S9 STEM image and HRTEM image of Pt/CNTs-CR@600.

Figure S10 STEM image and HRTEM images of Pd/CNTs-ECR catalyst.

Figure S11 STEM image and HRTEM images of Au/CNTs-ECR catalyst.

Figure S12 The optimized structures for Pt clusters on corresponding supports.

Figure S13 Calculated energies along the stretching pathway of the single Pt atom located on perfect hexagons to Pt_4 clusters. **Figure S14** The polarization curves of Pt/CNTs-ECR measured in old electrolyte and the fresh.

Figure S15 The polarization curves for five parallel samples activated under the same electrochemical conditions.

Figure S16 HER performances of four catalysts prepared under different conditions.

Materials

Chloroplatinic acid ($H_2PtCl_6·6H_2O$, 37.5%) was purchased from Aladdin Chemistry Co., Ltd. 5 wt% Nafion 117 solution was purchased from Sigma-Aldrich Chemistry Co., Ltd. $NaBH_4$ (AR, 96%) and sulfuric acid (H_2SO_4, >70%) were purchased from Sinopharm Chemical Reagent Co., Ltd. Multi-walled CNTs (MCNTs) (purity > 97%, diameter 20-50 nm, length > 2 μm) was purchased from Shenzhen Nanotech Port Co. Ltd. (China). The MWCNTs were donated as CNTs directly in the text. All the chemicals were used directly without further treatment otherwise stated.

Preparation of series of CNTs supports

CNTs: original CNTs were in 0.5 M H_2SO_4 at 80 °C for 8 h to remove impurities and washed with distilled water and ethanol till the pH approaching 7. The final material was labeled as CNTs.

CNTs@COOH: original CNTs was oxidized with 4 M HNO_3 and 4 M H_2SO_4 mixture solution at 80 °C for 8 h and then washed with distilled water till the pH approaching 7. The final material was labeled as CNTs@COOH.

CNTs@OH was purchased directly and the same model with CNTs. CNTs@OH was used directly without further treatments.

CNTs@700: CNTs@COOH support was treated with 700 °C pyrolysis for 4 h under high purity nitrogen atmosphere. The final material was labeled as CNTs@700.

Preparation of Pt-based electrocatalysts

Pt/CNTs-ECR: The Pt/CNTs-ECR catalyst was synthesized via a simple two-step method including the adsorption process and electrochemical activation processes. Typically, specific amount of CNTs and $H_2PtCl_6 \cdot 6H_2O$ aqueous was dispersed in deionized water in a beaker and treated under ultrasound for 30 min to reach saturated adsorption of $PtCl_6^{2-}$ species, then the mixture was repeatedly centrifuged and washed with deionized water until the remaining liquid without $PtCl_6^{2-}$. Then, the obtained black powder ($PtCl_x$/CNTs) was dried at 40 °C overnight. Avoiding the photolysis of $PtCl_6^{2-}$, all preparation process was operated under dark conditions. For the electrochemical activation process in 0.5 M H_2SO_4, the collected black powder will be confected into ink and subjected to the working electrode of a three-electrode system. A dramatically increased activity can be found with increasing times of repeated tests in electrolyte, a stable and prominent HER activity was acquired after several cycles. The activation process accompanied with the hydrogen generation. These pre-absorbed $PtCl_6^{2-}$ species on the CNTs are rapidly reduced to metallic Pt where the potential of hydrogen evolution occurred. The final catalyst was denoted as Pt/CNTs-ECR. The Pt/CNTs@H-ECR, Pt/CNTs@OH-ECR and Pt/CNTs@COOH-ECR electrocatalysts were prepared under the same conditions.

Pt/CNTs-CR : For the preparation of Pt/CNTs-CR catalyst, another 10 mL freshly prepared $NaBH_4$ solution (10 mg/mL) was added into the mixture suspension of CNTs and H_2PtCl_6 (the addition of amount was based on the actual Pt loading of Pt/CNTs-ECR), followed by another 30 minutes of ultrasonic treatment. Lastly, the mixture was washed and dried with the same process for Pt/CNTs-ECR.

Pt/CNTs-ED: Controlling the same concentration of H_2PtCl_6 in 0.5 M H_2SO_4 electrolyte aqueous as the preparation of $PtCl_x$/CNTs precursors. Pristine CNTs inks were coated on the working electrode of a three-electrode system. The electrochemical deposition of Pt nanoparticles on CNTs was displayed under the same activation process with the preparation of Pt/CNTs-ECR catalysts.

Pt/CNTs-ECR@600: The prepared Pt/CNTs-ECR catalyst was grinded and transferred into a 30 mL crucible and heated at a rate of 2 °C /min to 600 °C for 1 h in N_2 atmosphere.

Characterization

High resolution transmission electron microscopy (HRTEM) was conducted on JEOL-2100F to record the morphology and crystalline structures of Pt-based catalysts. The powder X-ray diffraction (XRD) patterns were collected on a D/max 2500VL/PC diffractometer (Japan) equipped with Cu Kα radiation.

The textural structures were studied by N_2 adsorption analysis using a Micromeritics ASAP 2020. The specific surface area and the pore size distribution (PSD) were calculated with the conventional Brunauer−Emmett−Teller (BET) method and the Barrett−Joyner−Halenda (BJH) algorithm, respectively. The Raman spectra were collected on a Raman spectrometer (JY, HR 800) using 514-nm lasers. The total content of Pt in the catalysts was determined by Inductively Coupled Plasma Atomic Emission Spectroscopy (ICP-AES, PerkinElmer Optima OES 8000). The samples were prepared by dissolving the samples in concentrated nitric acid in 200 $^{\circ}$C for 24 h.

Electrochemical measurements

The electrocatalytic performances of the Pt-based electrocatalysts were evaluated with a three-electrode electrochemical cell using a CHI760E electrochemical workstation. A Au foil and saturated calomel electrode (SCE) were used as the auxiliary and reference electrodes respectively. Typically, 4.0 mg Pt/CNTs-ECR catalyst was dispersed into a mixed solution containing 20 μL of 5wt % Nafion and 480 μL of anhydrous ethonal and treated with ultrasound for about 20 min to form a homogeneously dispersed ink. Then 5 μL of the catalyst ink was dropped onto the surface of a polished GC electrode (GCE, 5.0 mm diameter, 0.196 cm^2) and dried in air. The loading amount was calculated to be 0.14 mg cm^{-2}. The catalytic performance of all the reference catalysts were measured with the same catalyst loading. In order to enhance mass diffusion, commercial carbon cloth (1 cm × 1 cm, mass loading: 0.14 mg/cm^2) was also applied as the current collector of working electrode. For HER measurements, linear sweep voltammetry (LSV) was conducted with scan rate of 50 mV/s in 0.5 M H_2SO_4 as the activation process was not sensitive to the scan rate. All the used polarization curves are the steady-state one after several cycles. Electrochemical impedance spectroscopy (EIS) was carried out in potentiostatic mode from 100,000 Hz to 0.01 Hz. Cyclic voltammograms (CVs) under the same potential range with LSV was conducted to record the long-term durability. All the potentials in the electrochemical data in this work were converted to the potentials versus the reversible hydrogen elelctrode (RHE) based on the formula: E (vs. RHE) = E (vs. SCE) + E^0_{SCE} + 0.0592 pH. All the polarization data are without iR-correction.

The estimation of active sites density (n) and turnover frequency (TOFs)

The density of active sites for Pt-based electrocatalysts were quantitatively measured with underpotential deposition (UPD) method,[1] as the typical hydrogen adsorption/desorption peaks were seriously suppressed, the amount of 0.20 wt % Pt is beyond the level of detection. The Cu^{2+} reduction at an underpotential is more sensitive to the active sites for proton reduction than absorbed H.

In this approach, the number of active sites (n) was calculated based on the generated charges during the UPD copper (Cu) stripping (Q_{Cu}, $Cu_{upd} \rightarrow Cu^{2+} + 2e^-$).

The detailed calculation equation of active sites (n) and the turnover frequency (TOF, s^{-1}) are listed below:

(1) active sites: $n = Q_{Cu}/2\ F$,

(2) $TOF = I/(2nF)$,

where F (C mol^{-1}) is the Faraday constant, I is the current (A) at corresponding overpotential during linear sweep measurement, the factor 2 is the number of transferred electron based on that two electrons are required to form one hydrogen molecule ($2H^+ + 2e^- = H_2$).

The measurement of active sites density (n) was performed in a mixture solution of 0.5 M H_2SO_4 + 20 mM $CuSO_4$ + 60 mM NaCl. The addition of NaCl can effectively inhibit the overpotential deposition (OPD) due to the quick adsorption of Cl$^-$ on the Cu UPD adlayer. Basically, the deposition of copper was performed at various underpotential for 100 s in the mixture solution, then a liner voltammetric scan (10 mV/s) was carried out within the range of fixed potentials to ensure the full stripping of deposited Cu. The active site density can be estimated based on the charges exchanged during the oxidative stripping of the Cu UPD.

XAFS measurements and data processing

Pt L$_3$-edge XAFS measurements were performed at BL14W1 station in Shanghai Synchrotron Radiation Facility (SSRF). The electron storage ring of SSRF was operated at 3.5 GeV, with a maximum current of 250 mA. XAFS data were collected using a fixed-exit Si(111) double-crystal monochromator, and the energy was calibrated using metals foil. The samples were pelletized as disks of 13 mm diameter with 1 mm thickness by using LiF power as binder. Utilizing the ATHENA module of the IFEFFIT software packages, the obtained EXAFS data were performed according to the standard procedures.[2] The EXAFS contributions were separated from different coordination shells by using a hanning windows (dk=1.0 Å^{-1}). Subsequently, the quantitative curve-fittings were carried out in the R-space with a Fourier transform k-space range of 3.0-12.5 Å^{-1} using the module ARTEMIS of IFEFFIT. During the curve-fitting, the overall amplitude reduction factor S$_0^2$ was fixed to the best-fit value of 0.81 determined from fitting the data of metal Pt foil. For PtCl$_x$/CNTs, Pt/CNTs-ECR and Pt/CNTs-CR, the the structural parameters, such as the coordination number N, interatomic distance R, the Debye-Waller factor σ^2 and the edge-energy shift E$_0$ were allowed to vary during the fitting process. Fitting range: 1.0 Å-2.3 Å (PtCl$_x$/CNTs), 1.3 Å-3.2 Å (Pt/CNTs-ECR) and (Pt/CNTs-CR).

Computational Methods and Models

Theoretical Calculation part of this work was performed by using Vienna Ab-initio Simulation Package (VASP). Spin-polarized density-functional-theory calculation (DFT) with Perdew-Burke-Ernzerhof (PBE) implemented gradient approximation for the exchange-correlation functional. A plane wave

basis set with an energy cut off of 400 eV was chosen. The projector augmented wave (PAW) method proposed by Blöchl and implemented by Kresse was used to describe the electron-ion interactions.

A Monkhorst−Pack k-point mesh of $2\times2\times1$ was used as the Brillouin zone integration during the structure optimization and reaction pathway calculation. Pt clusters with 4 atoms was modeled for Pt/CNTs-ECR. The periodic condition was employed along the x and y directions. A vacuum region of 15 Å was set to avoid interactions between the periodically repeated slabs. The relaxation was stopped when the force residue on the atom was smaller than 0.02 eV/Å. The adsorption energy for the chemisorption of Pt_4 cluster is defined as

$E_{ads} = E_{tot} - E_{slab} - E_{Pt4}$

where E_{tot} is the total energy after Pt_4 cluster adsorption on the catalysts, E_{slab} is the energy of the clean catalyst alone, and E_{Pt4} is the energy of Pt_4 cluster alone.

The adsorption energy for the chemisorption of H is defined as

$E_{ads} = E_{tot} - E_{slab} - E_{1/2H2}$

where E_{tot} is the total energy after H adsorption on the catalysts, E_{slab} is the energy of the clean catalyst alone, and $E_{1/2H2}$ is the half energy of H_2 in the gas phase.

Reactive barrier for HER: The free energy of intermediate H* adsorption state based on the hydrogen adsorption strength. The detailed calculation equation is listed below:

$\Delta G_{H*} = \Delta E_{H*} + \Delta ZPE - T\Delta S$, where ΔE_{H*} is the bonding energy of H species, ΔZPE and ΔS are the zero point energy change and entropy change of adsorption H, respectively. Based on previous works, the calculation of ΔG_{H*} can be defined as

$\Delta G_{H*} = \Delta E_{H*} + 0.37$ eV
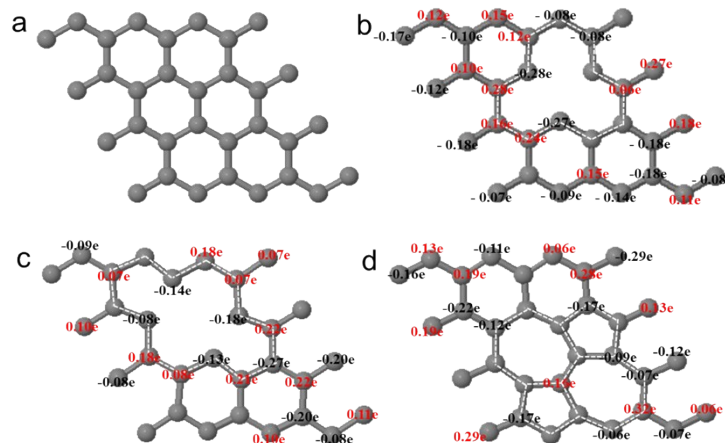
Figure S1 Charge distribution mapping of four types of carbon supports. (a) perfect hexagons, (b) Mono-vacancy, (c) Di-vacancy and (d) D5577 (Stone-Wales defects) structures. The perfect hexagons structure is electrically neutral. Atoms with charge polarization are labeled with corresponding charge states. Red and black numbers represent positive and negative charges respectively. As the low portion of defective structures within carbon skeleton, CNTs materials show electronegativity at the macro level.
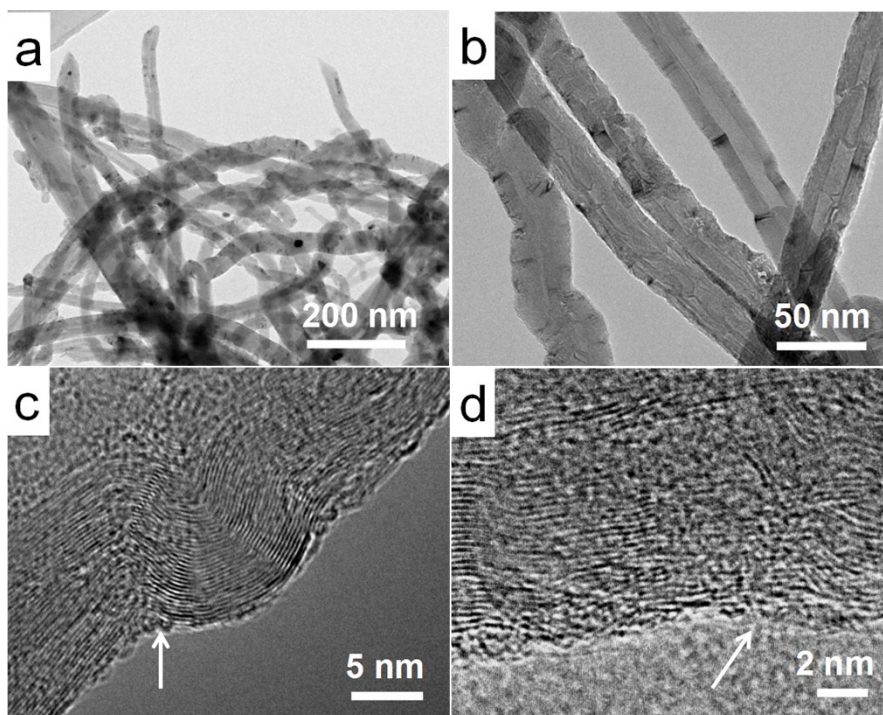
Figure S2 Morphology of pristine CNTs. TEM images (a, b) and HRTEM images (c, d) of CNTs. white arrows in (c, d) index the observed structural defects in pristine CNTs.
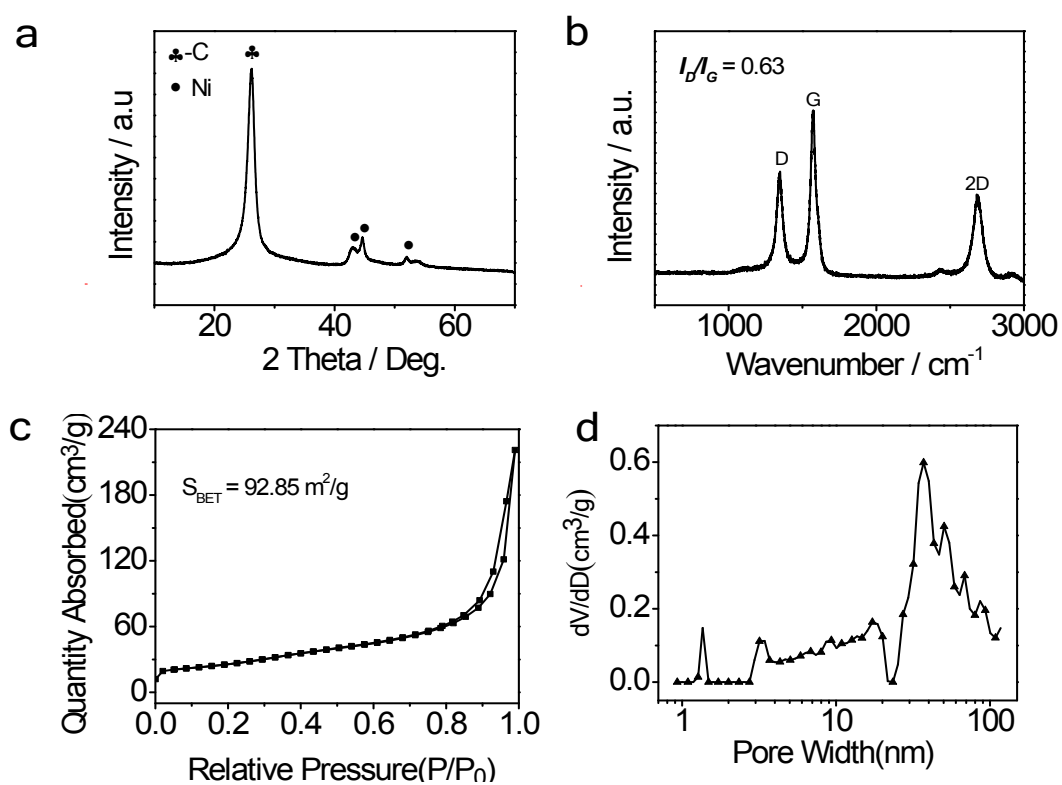
Figure S3 Textural properties of pristine CNTs. XRD pattern (a), Raman spectrum (b), N_2 adsorption isotherms (c) and the corresponding pore width distribution (d) of pristine CNTs.
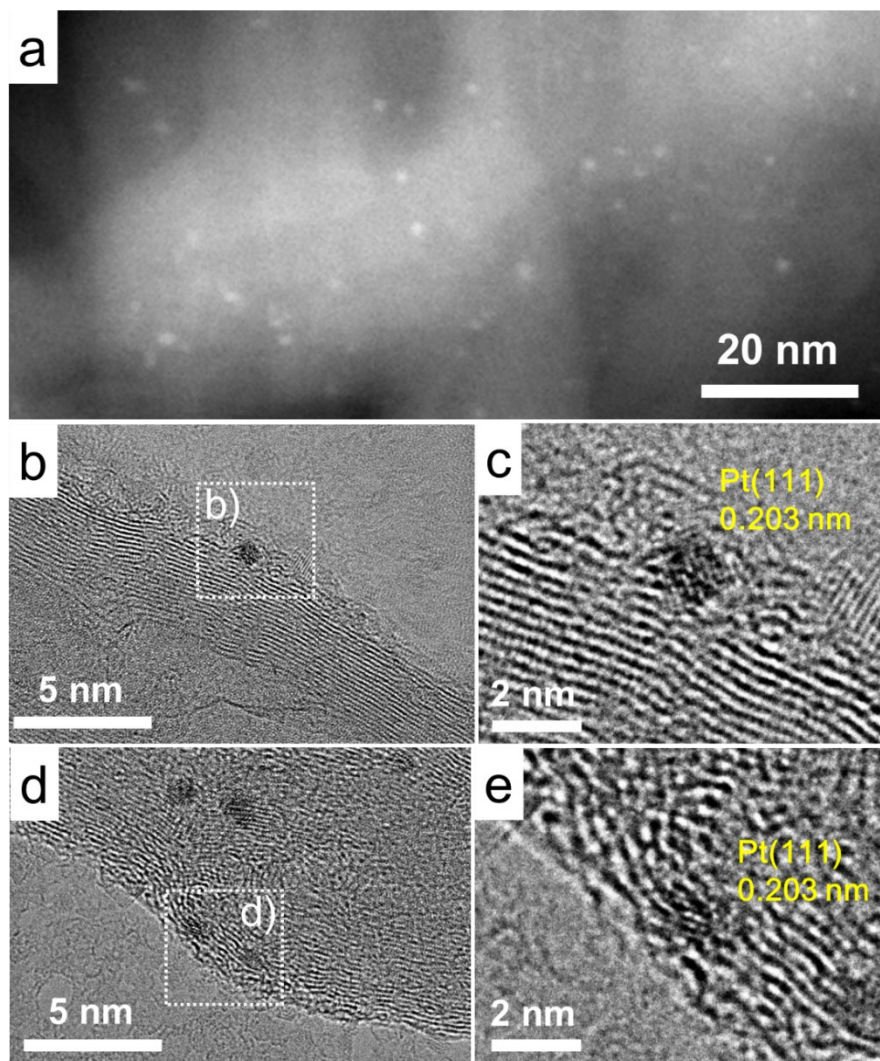
Figure S4 HAADF-STEM image (a) and HRTEM images of Pt/CNTs-ECR (b-e).
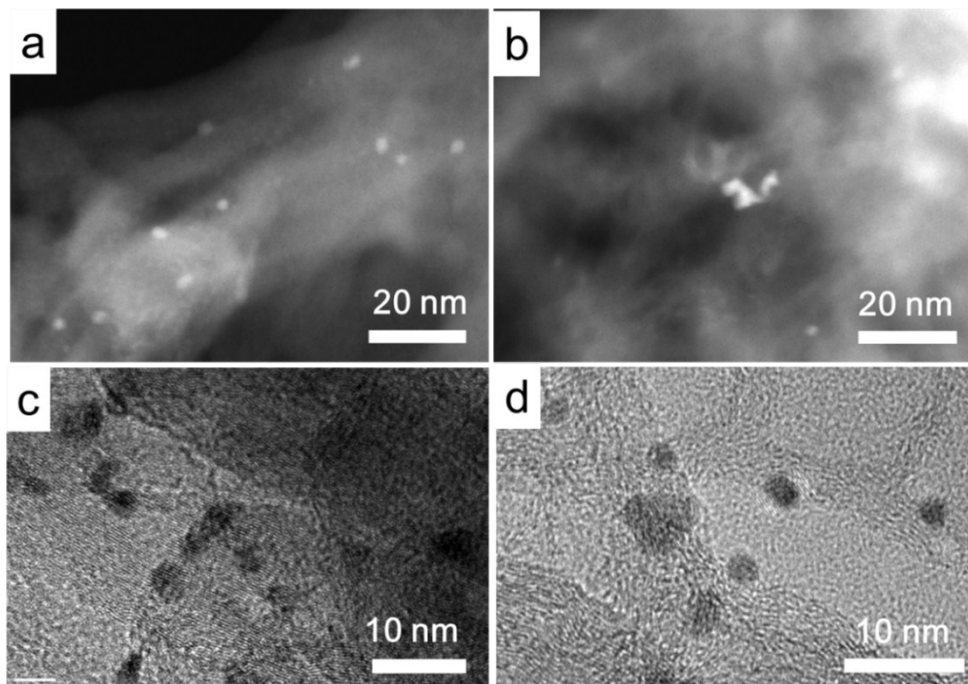
Figure S5 HAADF-STEM image (a, b) and HRTEM images of Pt/CNTs-CR (c, d)
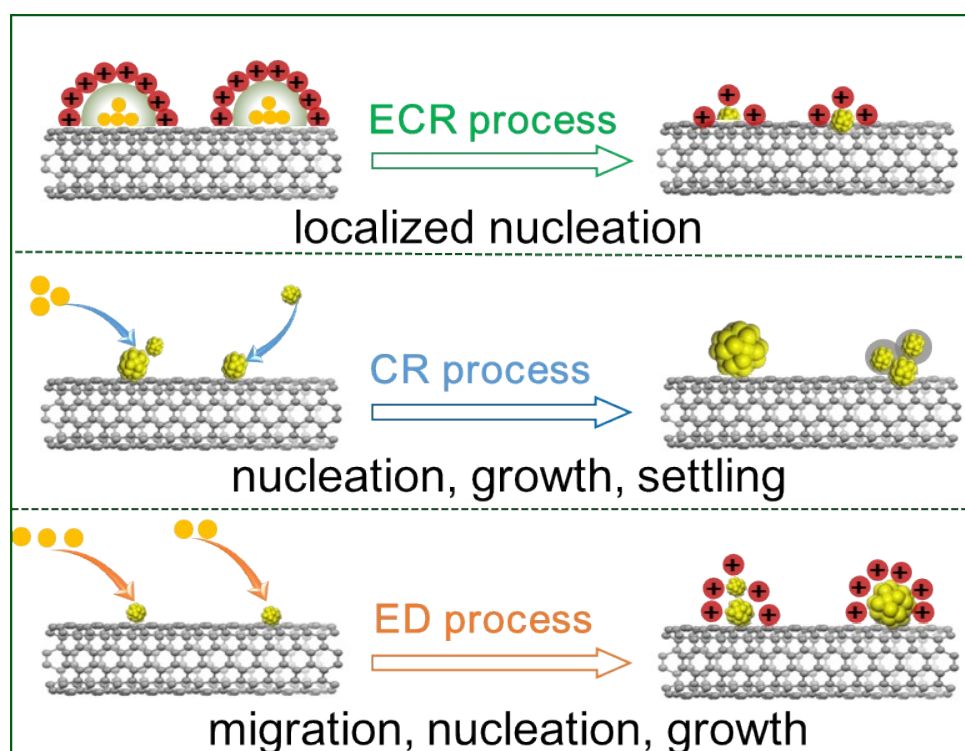
Figure S6 The proposed processes of Pt nucleation and growth for three different methods.
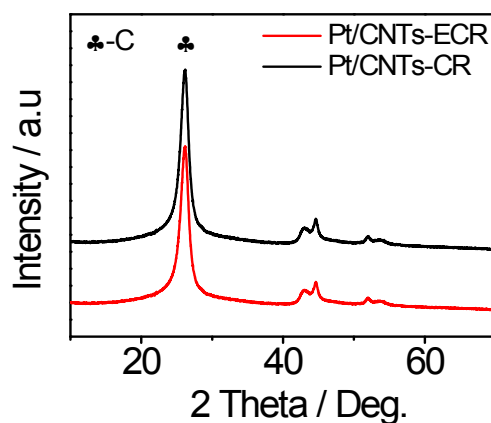
Figure S7 X-ray diffraction (XRD) analysis of Pt/CNTs-ECR and Pt/CNTs-CR.
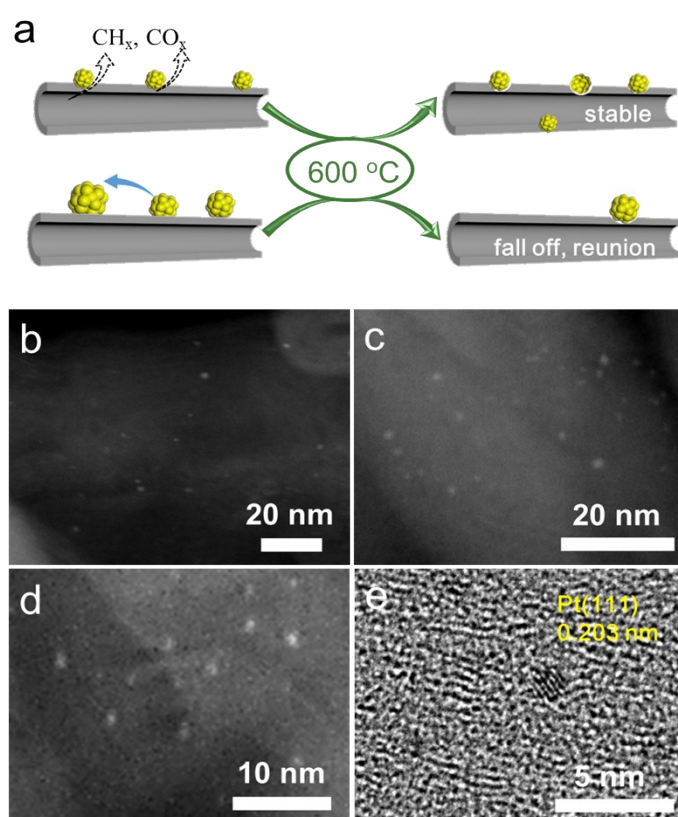
Figure S8 The thermal stability of Pt/CNTs-ECR. (a) A proposed model for the changes in Pt/CNTs-ECR and Pt/CNTs-CR catalysts after 600 °C treatment under inert atmosphere. STEM images (b-d) and HRTEM image (e) of Pt/CNTs-ECR@600.

The exceptional stability of Pt cluster in Pt/CNTs-ECR has been further demonstrated by performing high-temperature treatment at 600 °C under inert atmosphere. As seen in Figure S8, dispersed Pt clusters size with ~ 1 nm could be found clearly after treatment under 600 °C, revealing the good thermal stability of Pt/CNTs-ECR. Specifically, the high stability could be well explained as Pt cluster would corrode the surrounding defective carbon at high temperature and embedded itself into the formed holes. High thermal stability of

supported metal clusters is challenging, the advantageous feature of Pt/CNTs-ECR catalyst could broaden its practical application.
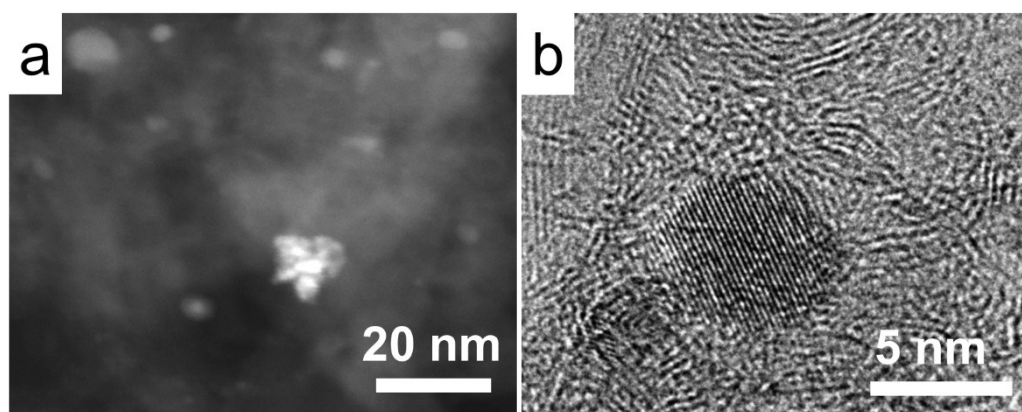
Figure S9 STEM image (a) and HRTEM image (b) of Pt/CNTs-CR@600.

In the Pt/CNTs-CR sample, some Pt NPs as large as 10~20 nm were observed. Due to the low melting point, Pt nanocrystal could be mobile under high-temperature, especially for unstable Pt NPs hanged on the external surface, and form agglomerative larger Pt crystals.
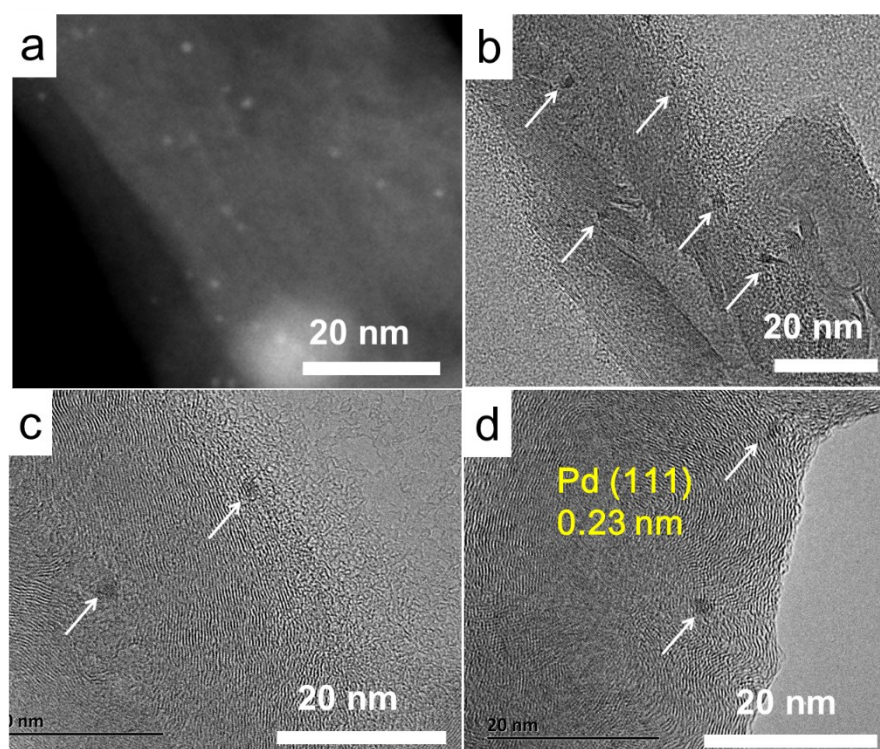
Figure S10 STEM image (a) and HRTEM images (b-d) of Pd/CNTs-ECR.
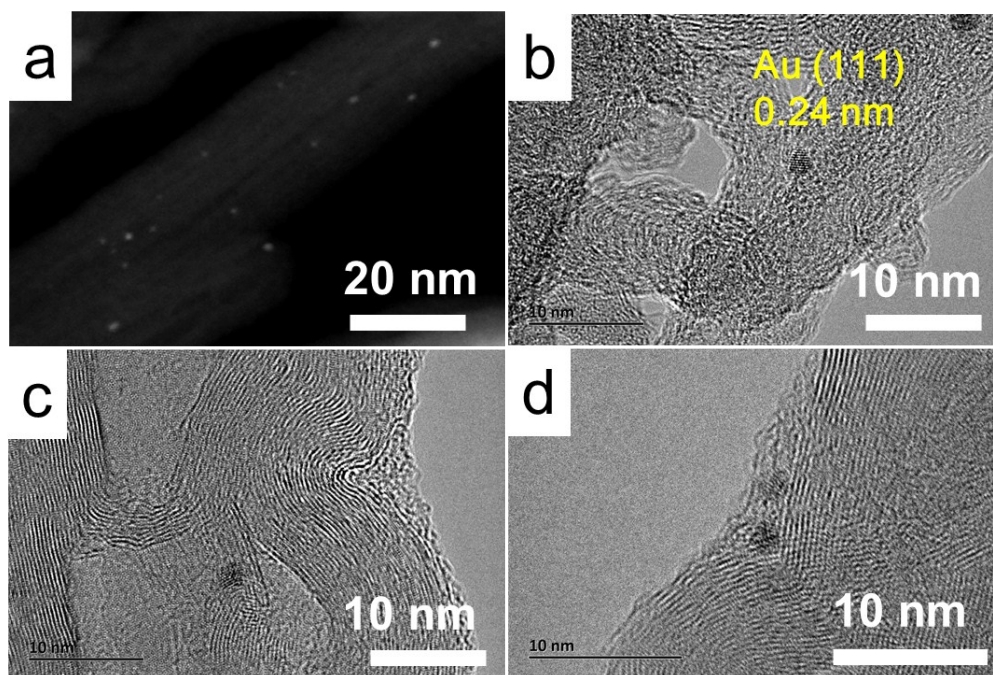
Figure S11 STEM image (a) and HRTEM images (b-d) of Au/CNTs-ECR catalyst.
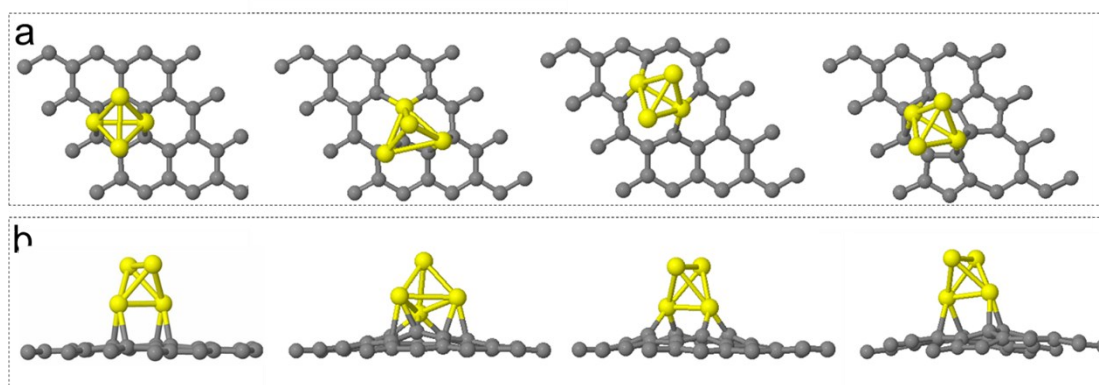
Figure S12 The optimized structures for Pt clusters on corresponding supports viewed from the top (a) and sides (b).
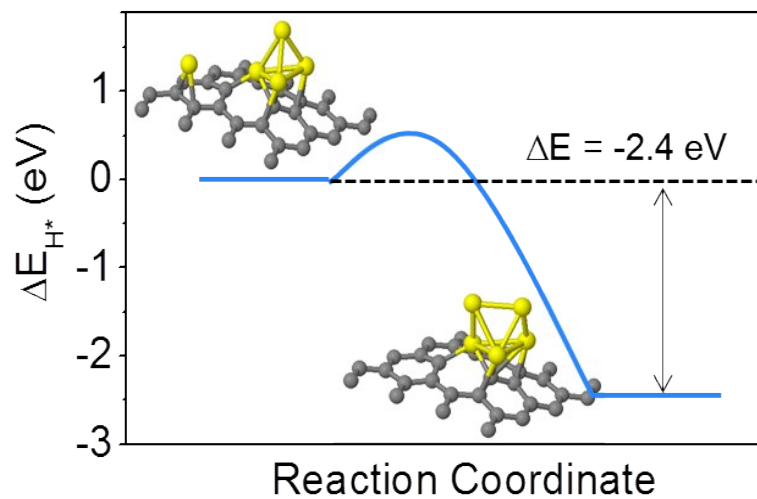
Figure S13 Calculated energies along the stretching pathway of the single Pt atom located on perfect hexagons to Pt$_4$ clusters trapped by Mono-vacancy defects and the corresponding initial and final configurations.
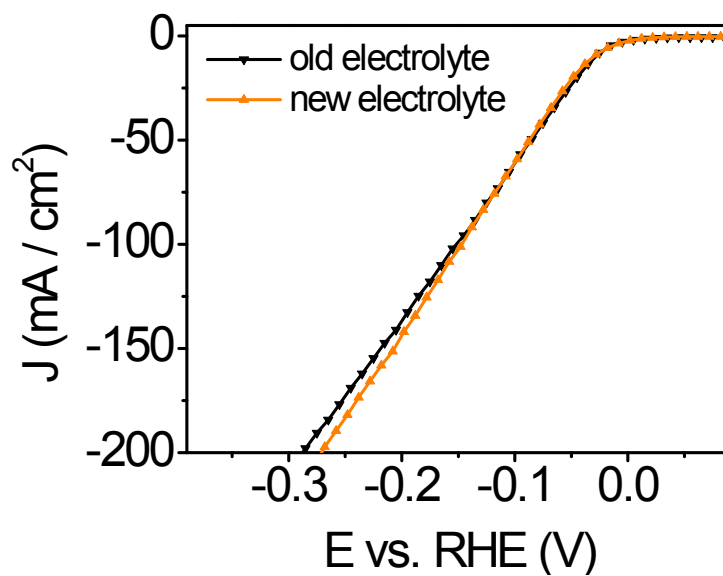
Figure S14 The polarization curves of Pt/CNTs-ECR measured in old electrolyte and the fresh.
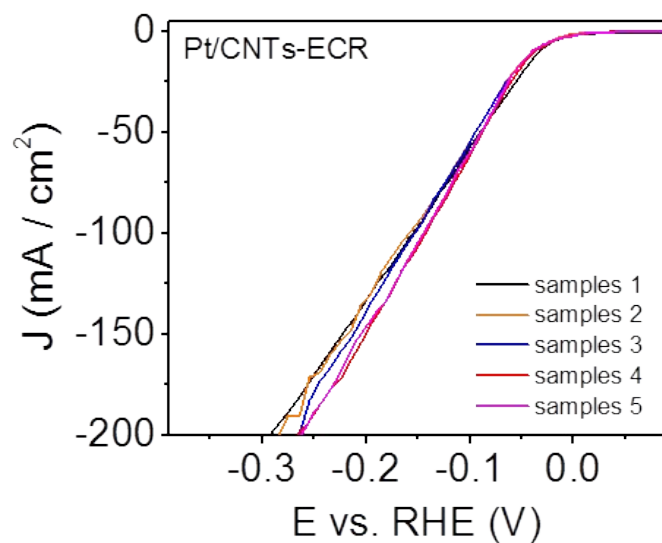
Figure S15 The polarization curves for five parallel samples activated under the same electrochemical conditions.
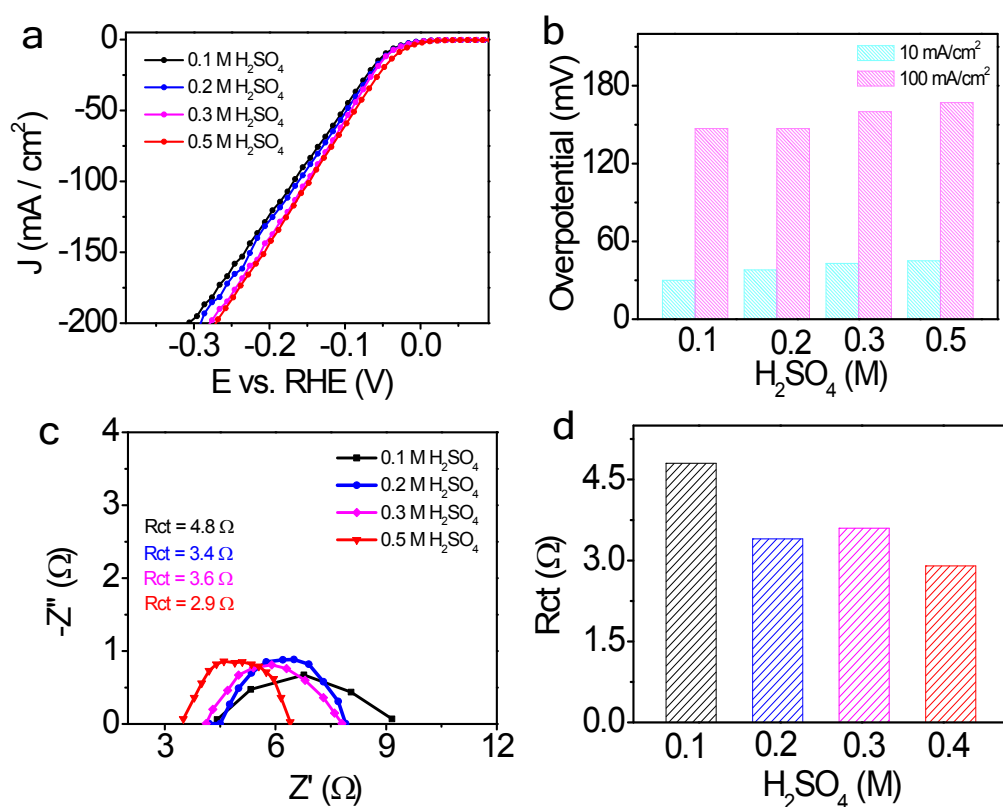
Figure S16 The polarization curves (a), overpotential at 10 mA/cm^2 (b) and Rct of four catalysts prepared under different conditions(c,d).

The hydrogen generation under acid media faced with the practical issue associated with the corrosion of

equipment and treatment of waste liquid. We also investigated the effect of electrolyte concentration on the reduced metallic Pt and compared their activity, aiming to reduce the acid concentration during preparation process. The Pt/CNT-ECR was activated under different concentration of electrolyte from 0.1 M to 0.5 M with K_2SO_4 act as the corresponding compensation ion to eliminate the resistance of ion migration. As shown in Figure S16, the four catalysts prepared under different conditions shown similar HER activity and reaction kinetics under 0.5 M H_2SO_4. This valuable result may drive down the preparation cost of catalyst.
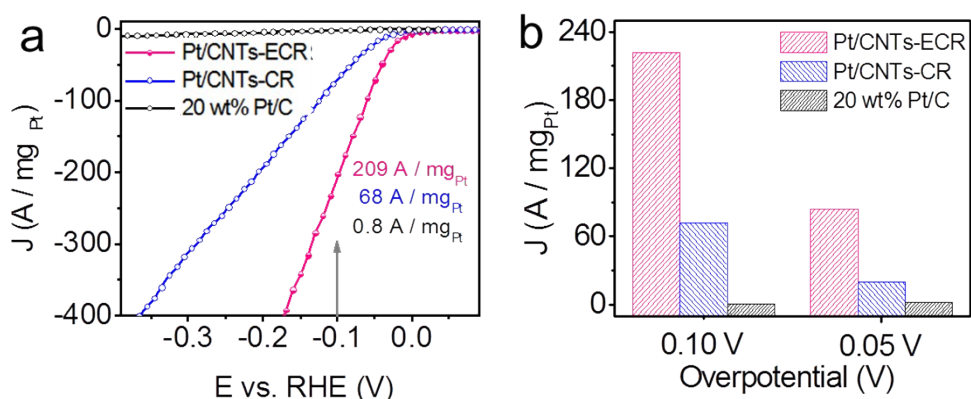
Figure S17 The comparison of mass activity. (a) The mass activity of Pt/CNTs-ECR, Pt-CNTs-CR and commercial Pt/C. (b) The comparison of mass activity at given voltammetry. Mass activity was normalized in reference to the real loading amount of Pt for these three catalysts.
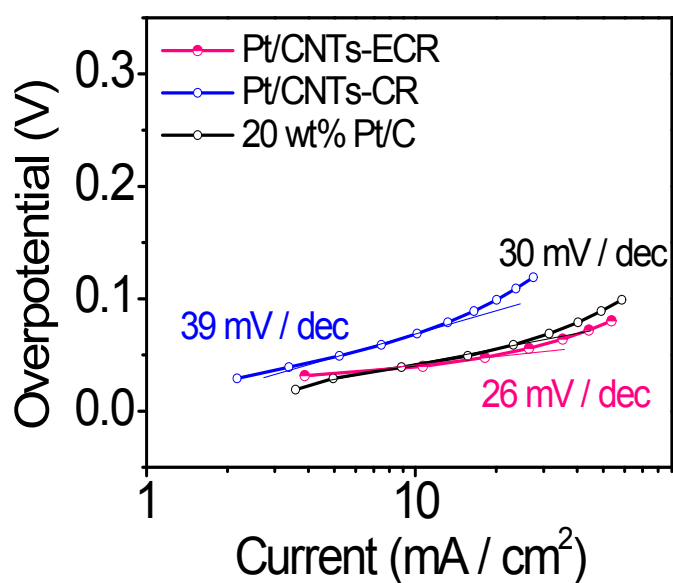
Figure S18 Tafel plots obtained from the corresponding polarization curves.
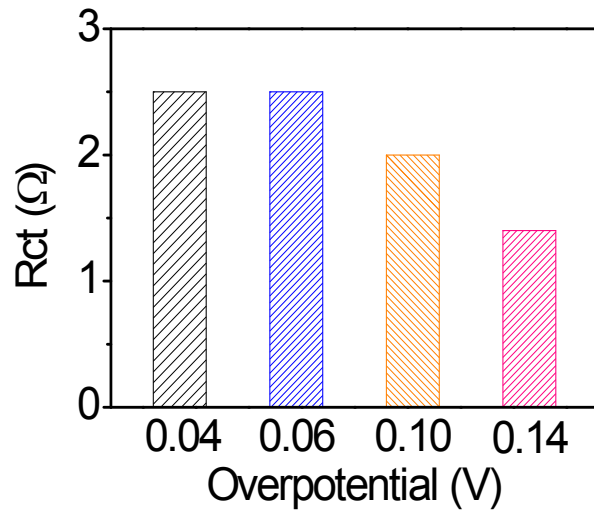
Figure S19 Charge transfer resistance (Rct) of Pt/CNTs-ECR catalyst under different voltages.
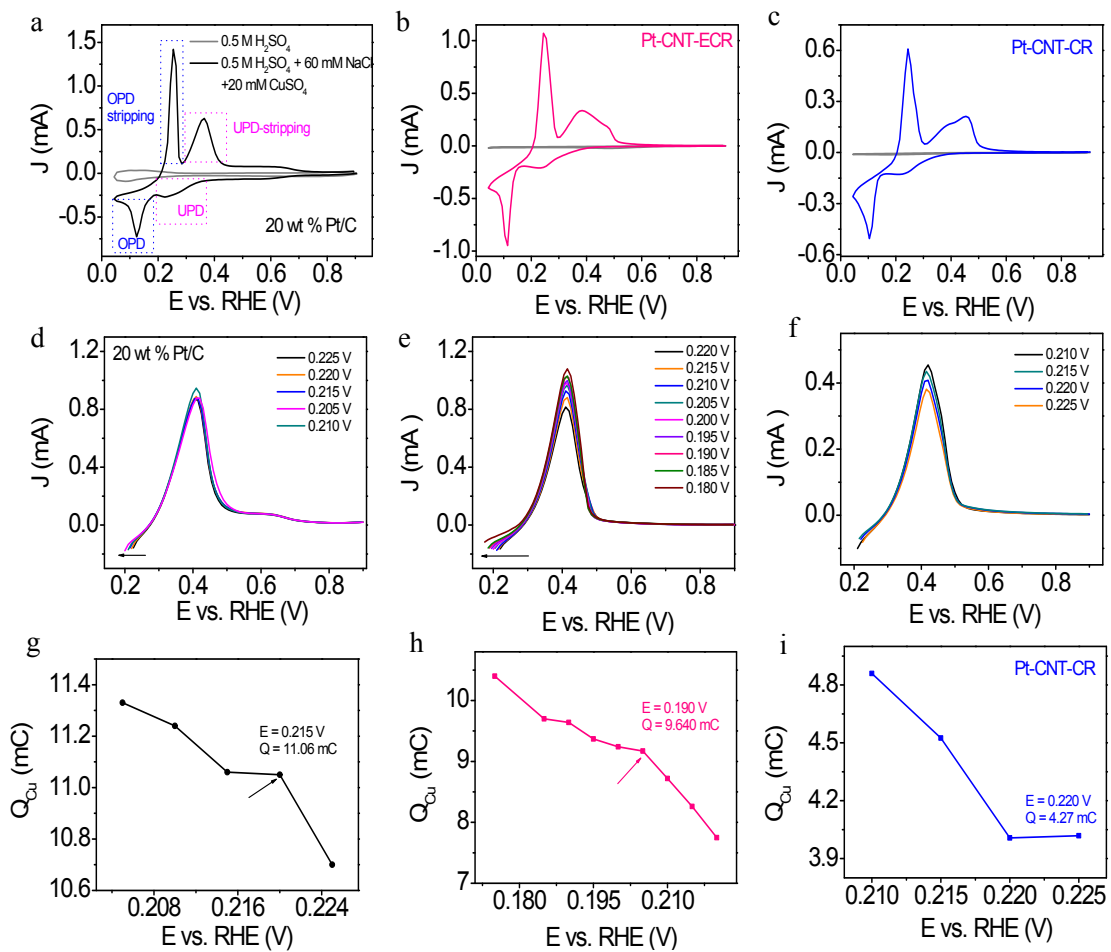
Figure S20 The measurements of active sites. The current–voltage scan for 20 wt% Pt/C (a), Pt/CNTs-ECR (b) and Pt/CNTs-CR (c) in different solutions. The corresponding charges required to strip the Cu deposited at different under potentials (d-f) and LSV curves under different initial voltages (g-i).
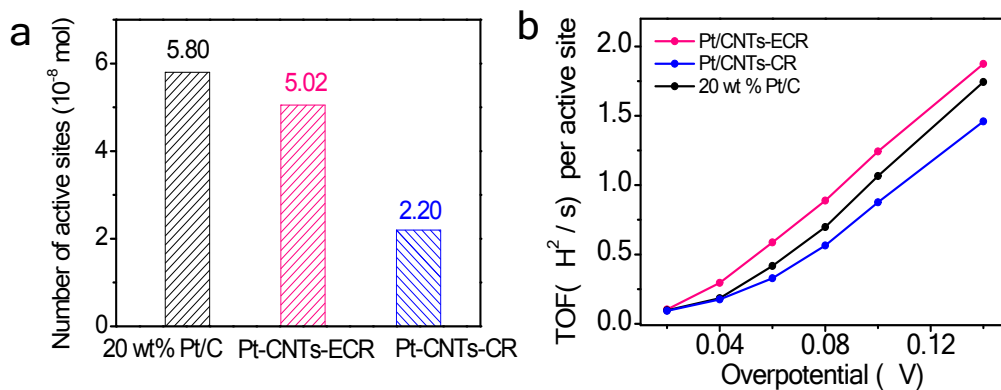
Figure S21 The comparison of active sites. (a) The number of active sites in 20 wt% Pt/C, Pt/CNTs-ECR and Pt/CNTs-CR measured with Cu-UPD method. (b) The relationship between TOF and the overpotential.
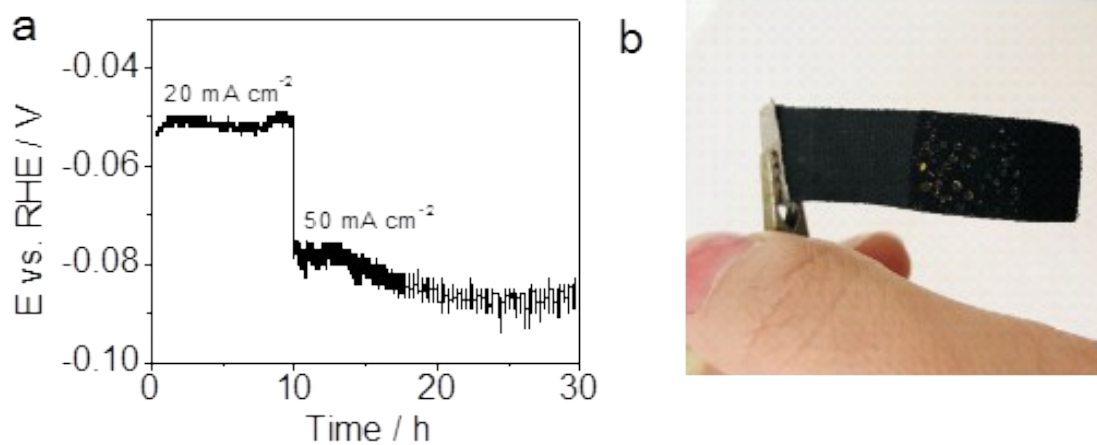
Figure S22 Stability of Pt/CNTs-ECR at large current density. (a) Long-term stability under high current density of 20 mA/cm^2 and 50 mA/cm^2. (b) Photographs of carbon cloth after 30 h operation.
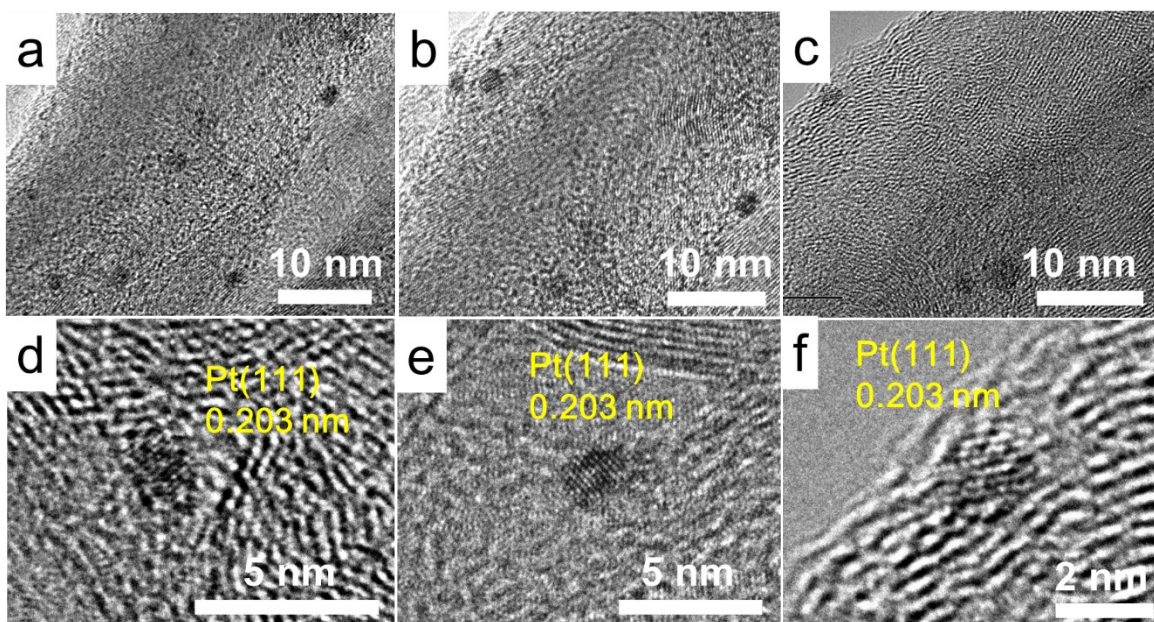
Figure S23 HRTEM images of Pt/CNTs-ECR after long-term stability in 0.5 M H_2SO_4.
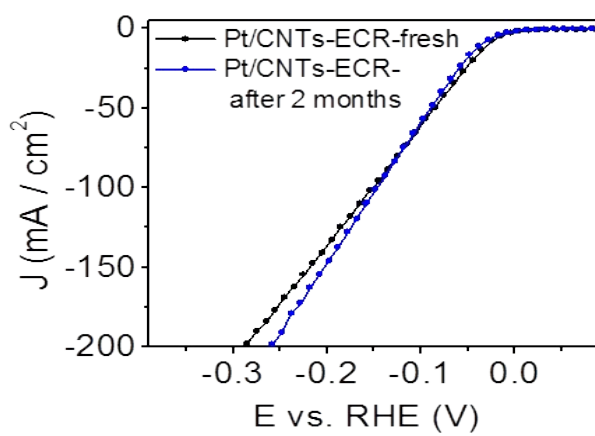
Figure S24 The activity of $PtCl_x$/CNTs after kept for two months.
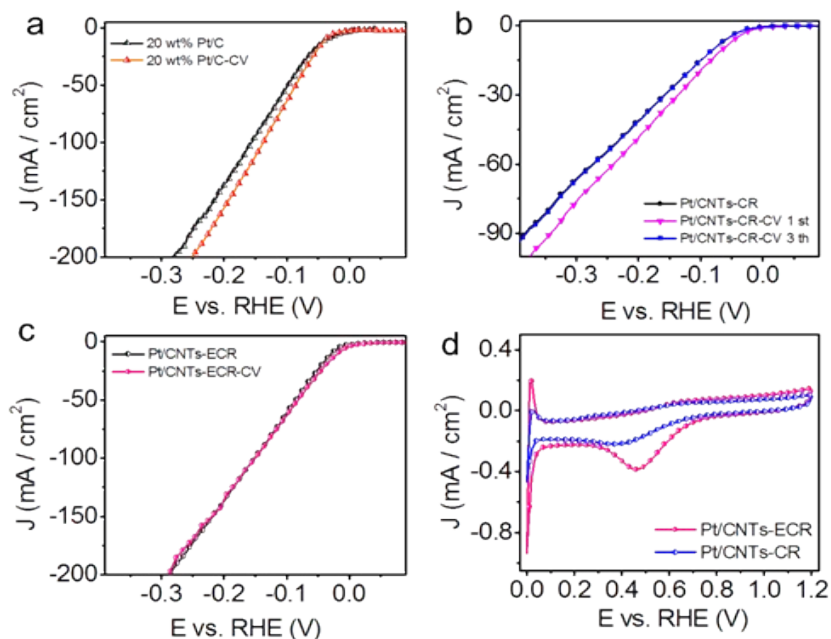
Figure S25 The CV activation of surfaces. The polarization curves of 20 wt% Pt/C (a), Pt/CNTs-ECR (b) and Pt/CNTs-CR (c) after CV activation. (d) the comparison of CV curves for Pt/CNTs-ECR and Pt/CNTs-CR.
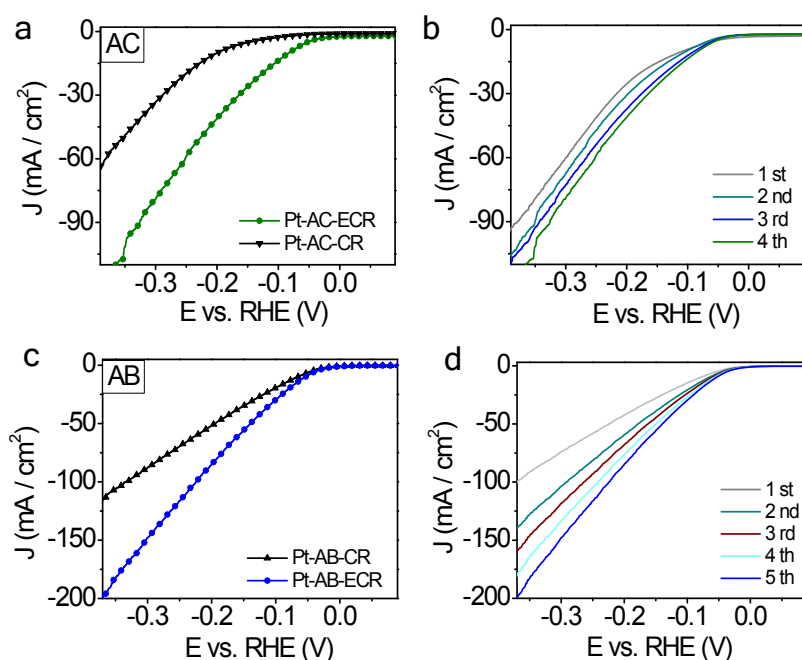
Figure S26 The activation process of Pt/AC-ECR and Pt/AB-ECR. Polarization curves of Pt/AC-ECR (a) and Pt/AB ECR (c) and their corresponding activation process (b), (d). AC (activated carbon) and AB (acetylene black) are the commercial porous carbon materials, assisting with porous adsorption of $PtCl_6^{2-}$ species. These results evidenced that higher activity of Pt formed under electrochemical conditions than that of chemical reduction.
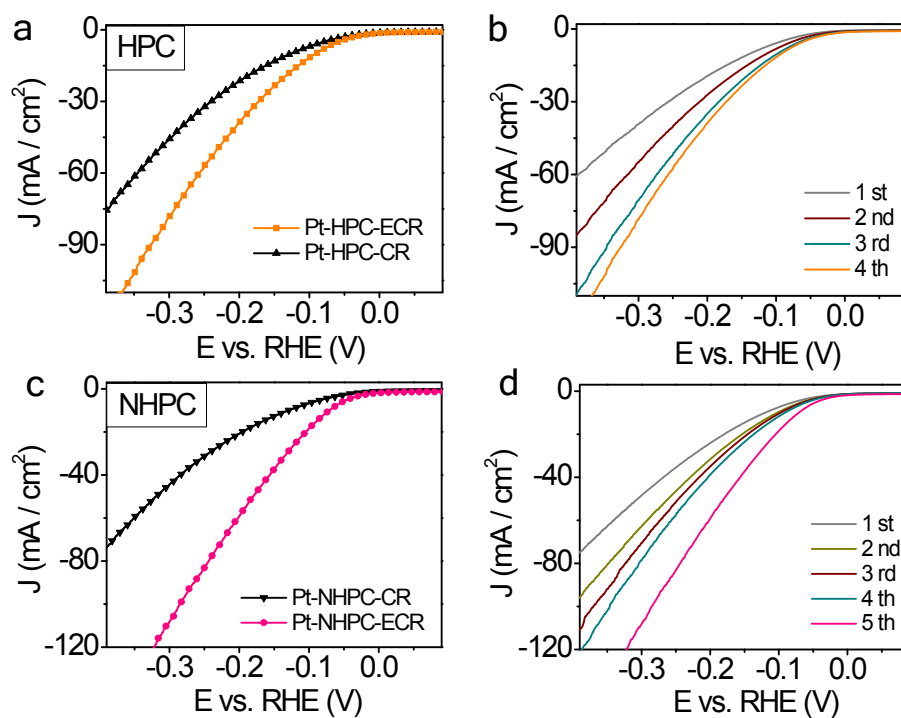
Figure S27 The activation process of Pt/HPC-ECR and Pt/NHPC-ECR. Polarization curves of Pt/HPC-ECR (a) and Pt/NHPC-ECR (c) and their corresponding activation process (b), (d).
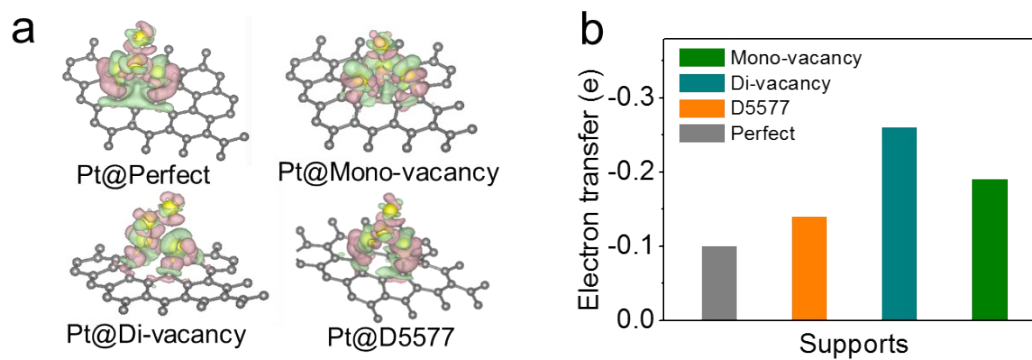
Figure S28 Charge density difference analysis for Pt clusters on four types of CNTs supports (a). The corresponding electron transfer between Pt clusters and carbon supports (b).
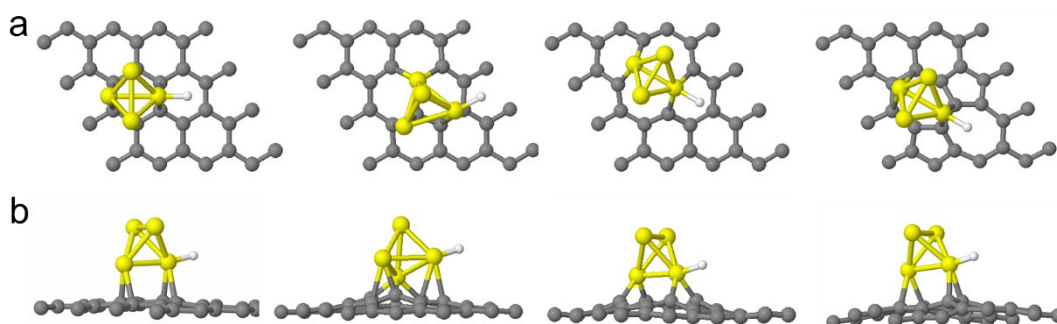
Figure S29 The optimized structures for H adsorption on corresponding supports viewed from the top (a) and sides (b).
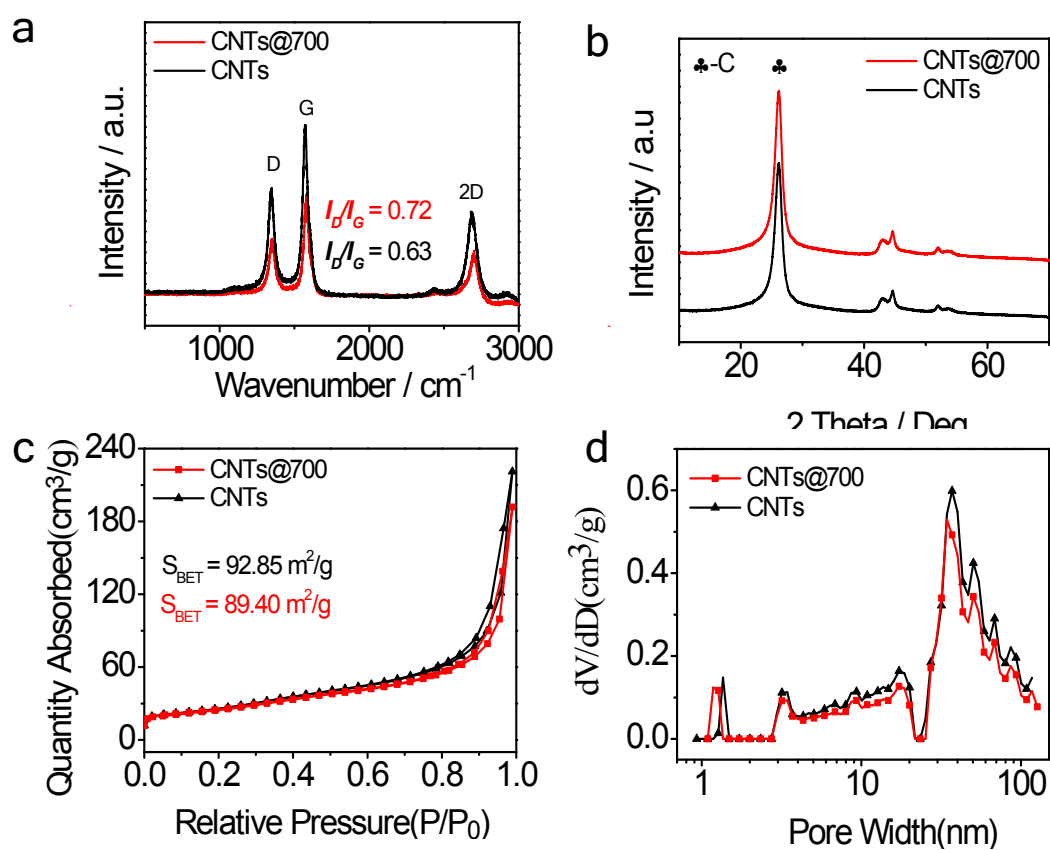
Figure S30 Textural properties of CNTs@700. Raman spectrum (a), XRD pattern (b), N_2 sorption isotherms (c) and the corresponding pore width distribution (d) of CNTs@700.
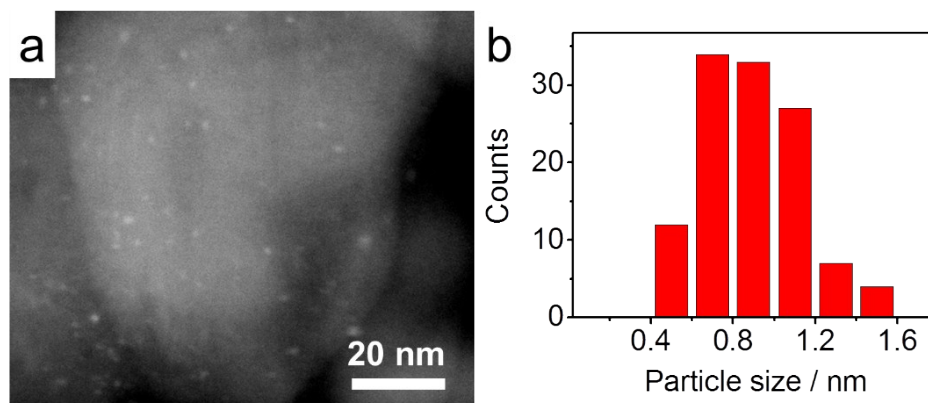
Figure S31 HAADF-STEM images of Pt clusters on Pt/CNTs@700-ECR catalyst.
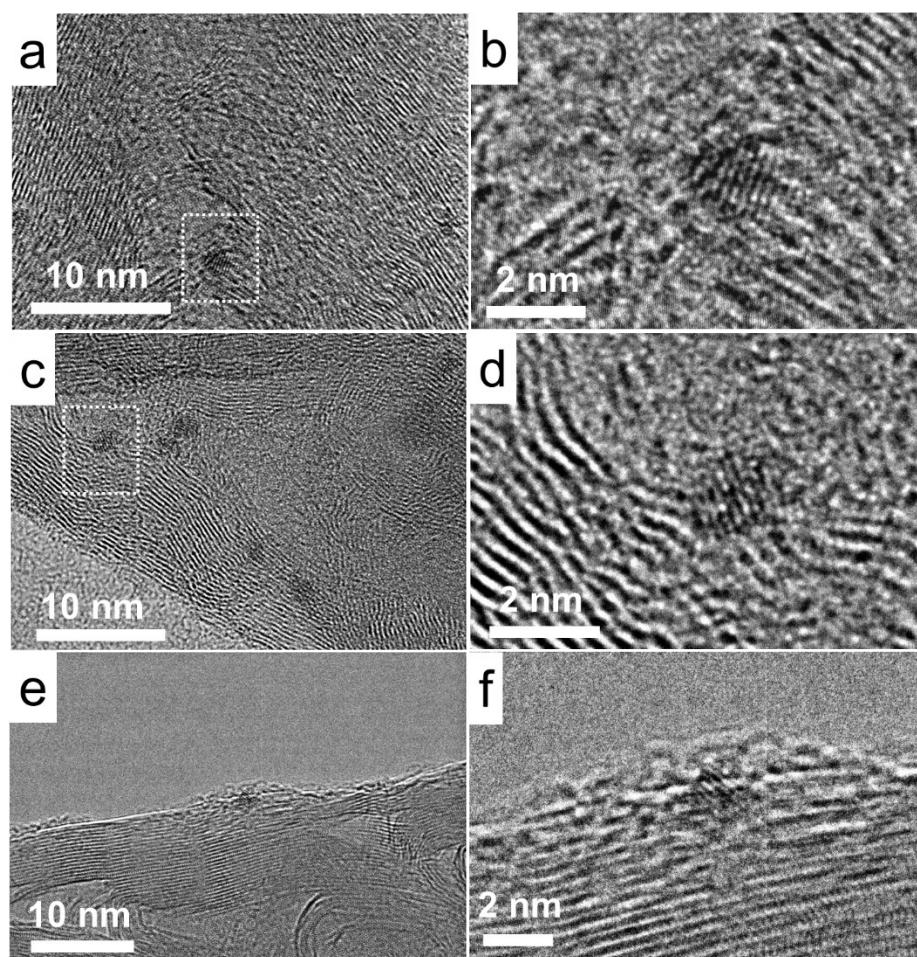
Figure S32 HRTEM images of Pt/CNTs@700-ECR.
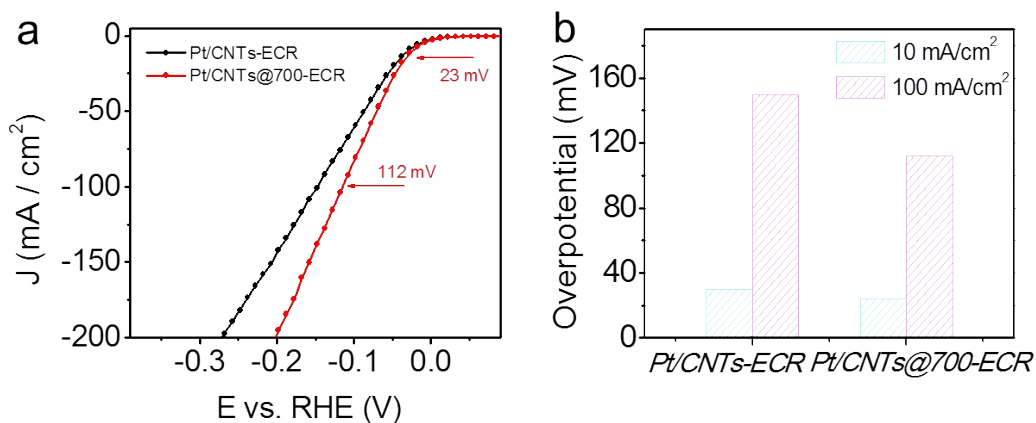
Figure S33 Polarization curves of Pt/CNTs-ECR and Pt/CNTs@700-ECR (a) and corresponding overpotential at 10 mA/cm^2 and 100 mA/cm^2 (b).
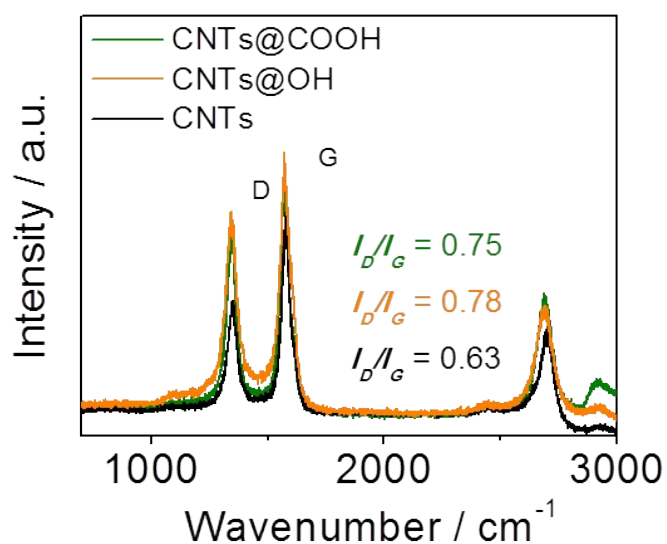
Figure S34 Raman spectrum of CNTs, CNTs@COOH and CNTs@OH.
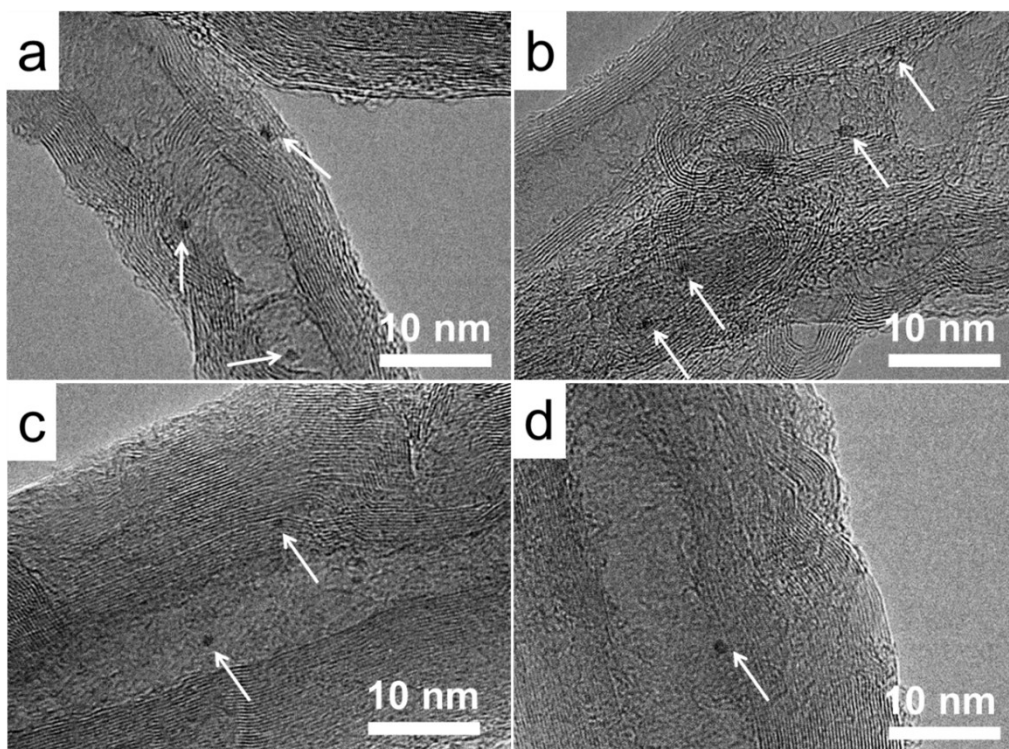
Figure S35 HRTEM images of Pt/CNTs@OH-ECR.
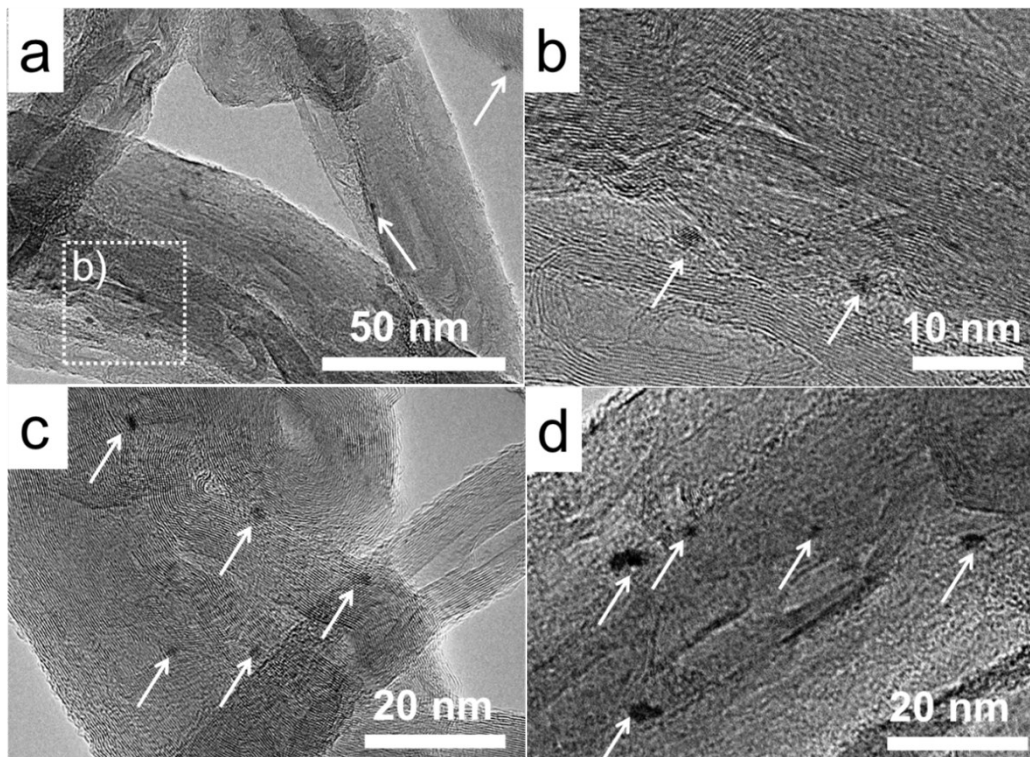
Figure S36 HRTEM images of Pt/CNTs@COOH-ECR.
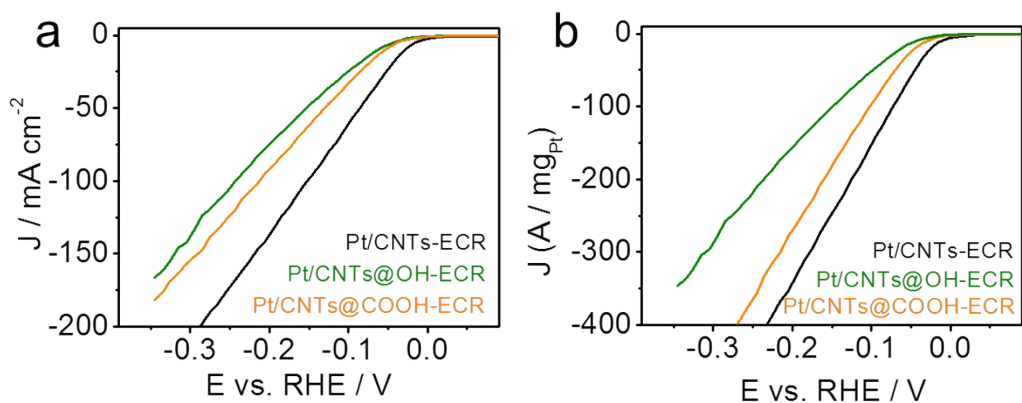
Figure S37 Polarization curves of Pt/CNTs@OH-ECR and Pt/CNTs@COOH-ECR (a) and their corresponding mass activity (b).

Table S1. Textural properties of the catalysts.

Sample	S_{BET}[a] [m² g⁻¹]	V_{total}[b] [cm³ g⁻¹]	$V_{Micropore}$[c] [cm³ g⁻¹]	$V_{mecro\&meso}$ [cm³g⁻¹]	$d_{Average}$[d] [nm]
CNTs	92.85	0.35	---	0.348	13.26
CNTs@700	89.40	0.30	0.002	0.298	12.70

[a] Brunuaer–Emmett–Teller surface area. [b] Calculated by single-point adsorption at relative pressure of 0.98. [c] Calculated by V–t plot method. [d]Calculated by BJH method from the desorption isotherm linear plot.

Table S2. The Pt content (wt%) analyzed by ICP-AES

entry	catalyst	ICP (wt%)
1	Pt/CNTs-ECR	0.35
2	Pt/CNTs-ECR[a]	0.30
3	Pt/CNTs-CR	0.21
4	Pt/CNTs@H-ECR	0.34
5	Pt/CNTs@COOH-ECR	0.22
6	Pt/CNTs@OH-ECR	0.19
7	20 wt%Pt/C	19.0

a: ethanol used as the solvent during the preparation of absorption.

Table 3. Pt L_3-edge fitting parameters

Sample	shell	N	R (Å)	DE_0 (eV)	$\sigma^2(10^{-3}Å^2)$	R-factor
Pt	Pt-Pt	12.0	2.79			
PtCl$_x$/CNTs	Pt-Cl	4.4±0.4	2.30±0.01	9.9±1.1	3.0±1.0	0.01
Pt/CNTs-ECR	**Pt-C**	3.0±0.8	2.21±0.02	13.3±2.5	3.4±3.5	0.01
	Pt-Pt	7.0±1.2	2.76±0.01	7.7±1.6	5.7±1.0	
Pt/CNTs-CR	**Pt-O**	0.9±0.2	2.00±0.02	10.5±2.0	3.5±2.4	0.007
	Pt-Pt	8.1±0.6	2.74±0.01	7.3±0.5	7.0±0.5	

N, coordination numbers; R, the internal atomic distance; σ^2, Debye-Waller factor; E_0, the edge-energy shift.

Reference

(1) Wang, J.; Wei, Z.; Mao, S.; Li, H.; Wang, Y., *Energ. Environ. Sci.,* 2018**, 11**, 800-806.

(2) YU Hai-Sheng, W. X.-J., LI Jiong, GU Song-Qi, ZHANG Shuo, *Nucl. Sci. Tech.,* 2015**, 26**, 50102-050102.